LA-6052-MS

c.3

Special Distribution
Reporting Date: August 1975
Issued: March 1976

LASL Participation in the Gas Explosive Simulation Technique Experiments

by

R. C. Carlos
R. A. Jeffries
E. M. Jones
J. L. Norton
H. M. Ruppel

los alamos
scientific laboratory
of the University of California
LOS ALAMOS, NEW MEXICO 87545

UNITED STATES
ENERGY RESEARCH AND DEVELOPMENT ADMINISTRATION
CONTRACT W-7405-ENG. 36

Work supported by the Defense Nuclear Agency.

LASL PARTICIPATION IN THE GAS EXPLOSIVE SIMULATION TECHNIQUE EXPERIMENTS

by

R. C. Carlos, R. A. Jeffries, D. M. Jones,

J. L. Norton, and H. M. Ruppel

ABSTRACT

Three of the Gas Explosive Simulation Technique experiments conducted by the Air Force Weapons Laboratory during November 1973 were observed optically. Dimensional and radiometric reduction of data recorded in the visible, near-infrared, and infrared spectral regions resulted in diameters, altitudes, and peak brightness temperatures that were compared with 2D hydrodynamic calculations. We found good agreement between the observations and the YAQUI computations.

I. INTRODUCTION AND SUMMARY OF RESULTS

In a cooperative effort with the Air Force Weapons Laboratory (AFWL), Kirtland AFB, Groups J-10 and T-3 of the Los Alamos Scientific Laboratory (LASL) participated in the experimental observation and theoretical analysis of three Gas Explosive Simulation Technique (GEST) experiments conducted during November 1973. The GEST experiments, designed to simulate atmospheric nuclear weapons effects, were performed in Coyote Canyon, south of Manzano Base, Albuquerque, NM.

In the period following the Limited Nuclear Test Ban, the requirement for the Energy Research and Development Administration (ERDA) laboratories to provide the defense community with more complete descriptions of nuclear weapons effects has continued in the absence of actual atmospheric tests. Complex numerical computer programs have been built to predict these effects, many of which were unrecognized at the time of the test ban. Also, numerous laboratory and field experiments have been designed to simulate specific features of these weapons effects and to verify the ability of various computer codes to describe the observed effects.

The performance of the GEST experiments by AFWL gave LASL the opportunity to observe a new simulation technique and to compare the results with theoretical output from existing computer codes. Designed primarily to simulate the late-time hydrodynamic behavior of a nuclear explosion in the atmosphere, GEST used large balloons that were filled with explosive methane and oxygen mixtures and centrally detonated. Three explosions were observed: a 1.8-m-diam rubber balloon (RB) with a 26-MJ predicted yield and two 9.7-m-diam Mylar balloons, MB-1 and MB-2, with 4-GJ predicted yields.

Optical observations in the visible and infrared spectral regions were made at a site 457.3-m ground range from the subevent

point. Although data were obtained for all three events, our analyses has been primarily confined to the larger MB-1 and MB-2 explosions. After reviewing the data, the six immediate conclusions are:

(1) Fireball and cloud dimensions measured in the photographic visible and near-infrared agreed reasonably well with similar measurements made at 5 and 10.5 μm during the first 10 s. Differences observed could be attributed to operator adjustments or data reduction techniques.

(2) The gross geometric properties of MB-1 and MB-2, i.e., altitude, diameter, balloon fragment cloud, etc., were virtually identical through the first 20 s. However, the morphologies of the two clouds were entirely different; MB-1 formed a "picture book" torus, whereas MB-2 formed an amorphous blob.

(3) The LASL 2D hydrodynamic program YAQUI successfully predicted the detailed behavior of MB-1.

(4) Peak brightness temperatures measured by two infrared framing instruments, one with peak sensitivity at 5 μm and one at 10.5 μm, were in excellent agreement.

(5) The peak temperature predicted by YAQUI at early times agreed with that measured with the infrared instrumentation. Differences at later times between theoretical and experimental temperature data are easily reconciled by considerations of the cloud's optical thickness.

(6) YAQUI was designed to calculate much larger explosions. Agreement between the YAQUI results and the GEST experimental data supports confidence in the programming inherent to YAQUI and in the ability of gas-filled balloons to simulate certain hydrodynamic nuclear weapons effects.

In Sec. II, we describe the photographic instrumentation and compare the spatial measurements with computed predictions. In Sec. III, we describe the infrared instrumentation and report the experimental spatial and temperature measurements. In Sec. IV, we describe the YAQUI program and its application to the low-yield GEST experiments. The Appendix contains infrared and visible images of MB-1 and MB-2.

II. PHOTOGRAPHIC AND TELEVISION INSTRUMENTATION AND RESULTS

The photographic instrumentation was used to record the gross dimensional features of the explosions. Two cameras, a pulsed model CA-75 and a fast-framing Mitchell, were used. The CA-75, installed on a fixed optical mount and with its wide field-of-view, recorded cloud altitude data. The Mitchell, on a tracking optical mount and with a smaller field-of-view, recorded cloud dimensions.

The tracking system installed in the diagnostic trailer was identical to those now used in the ERDA/USAF NC-135 aircraft. The system is capable of pointing accuracy near 0.1° and of driving up to 14 individual tracking mounts; here only 4 mounts were used. An operator observed the GEST events in real time using the IRV-1 Vidicon television system (spectral sensitivity 0.8-1.1 μm) and manually controlled the instrument pointing. Table I gives operational details of the optical instrumentation.

Using standard techniques developed for analysis of nuclear weapons effects, the photographic data were reduced by EG&G Inc., Los Alamos Operations. The results for the two larger events are shown in Figs. 1 and 2. Also shown are the results predicted by YAQUI. The theoretical and experimental results show excellent agreement.

III. INFRARED IMAGING INSTRUMENTATION AND RESULTS

We used three infrared imaging cameras, manufactured by the AGA Corporation, Sweden, to observe the GEST explosions. Two Model 680 cameras were operated at 16 fps. One had an InSb detector whose maximum sensitivity was near 5 μm (SAGA); the other had a HgCdTe detector that was most sensitive near 10.5 μm (LAGA). The third camera (BAGA), a Model 750 also with an InSb detector, was

TABLE I

PHOTOGRAPHIC AND TELEVISION INSTRUMENT PLAN

Camera	Framing Speed (fps)	Exposure		Aper	FL (mm)	Field H/V (mr)	Filter	Aiming H°/V°	Time Marker	Film				Event
		Shutter	Time (ms)							Size (mm)	Length (ft)	Type	Perf. No.	
CA-75	4		20	0.95	50	493/683	ND3.2 + W-12	0 20	Clock	35	100	EKIR	147000 147001 147002	RB MB-1[a] MB-2[b]
Mitchell	50	90°	5	16	180	136/102	W-89B	Tracked	100 PPS	35	400	2480	147006 147007 147008	RB MB-1
IRV-1	30	-	-	5	30-300 Zoom	40/33[a]	7-56	Tracked	World time	-	-	Video Tape	RB	RB MB-1 MB-2

[a]MB-1, 11/28/73, 16:38:40 UT.

[b]MB-2, 11/30/73, 15:30:08 UT.

[c]At 300-mm FL.

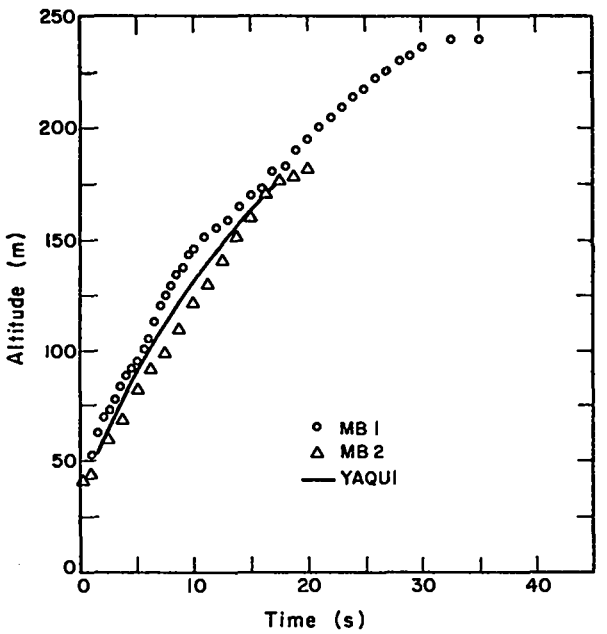

Fig. 1. Altitude measured from visual camera records for MB-1 and MB-2 and calculated by YAQUI.

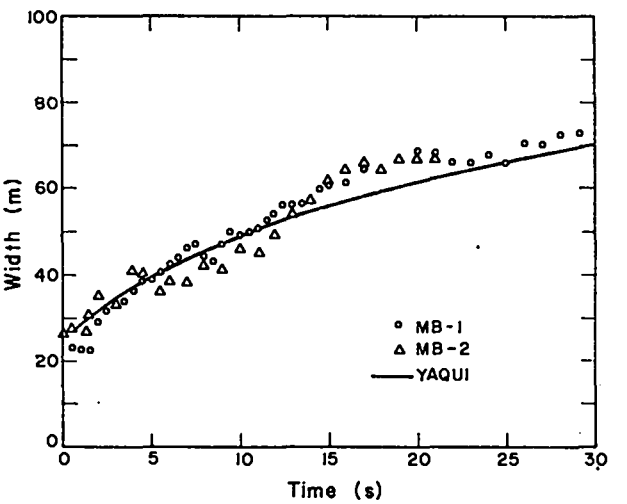

Fig. 2. Cloud diameter from Mitchell camera records compared with YAQUI predictions.

operated at 25 fps in an ac-coupled mode that precludes absolute calibration. All were mounted on trackers and followed the ascent of the clouds.

Cloud diameters extracted from the infrared records are presented in Figs. 3 and 4. Comparison with the optical results (Fig. 2) shows general agreement, but also some interesting differences. The most important differences show the distribution of hot, emitting gas observed by SAGA and LAGA vs the distribution of material that scattered sunlight and was recorded photographically. At 5 and 10.5 μm, scattered sunlight makes a negligible contribution. After ∿ 3 s, thermal radiation from hot gas was negligible in the visible and near-infrared wavelength bands. At early

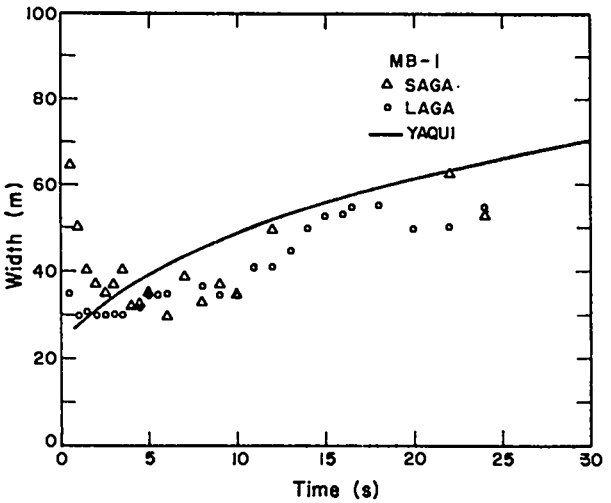

Fig. 3. Cloud diameters for MB-1, as determined from infrared cameras, compared with YAQUI predictions.

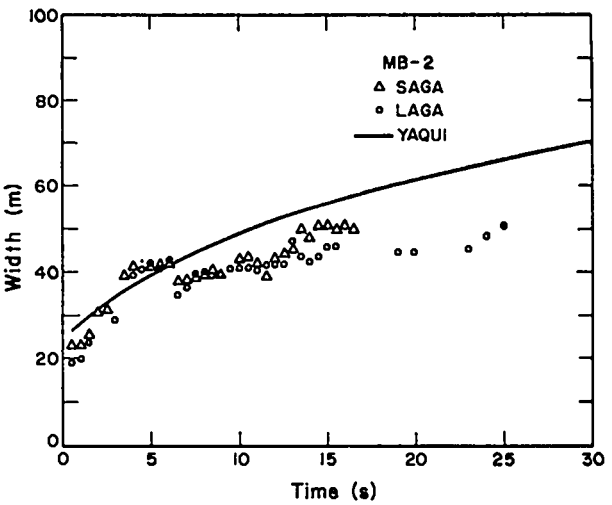

Fig. 4. Cloud diameters for MB-2, as determined from infrared cameras, compared with YAQUI predictions.

times for the MB-1 experiment ($t < 3$ s), the dynamic range of the infrared instruments was too small, resulting in artificially large, saturated images. Between 3 and 15 s, the visible and infrared diameters are similar. After 15 s, the infrared images are smaller, suggesting that the gas emitting above threshold levels was more concentrated than the scattering material.

For MB-2, the infrared dimensions are in good agreement both with the photographic data at early times and with the infrared results from MB-1 at later times.

Maximum brightness temperature histories were obtained from the SAGA (5-μm) and LAGA (10.5-μm) records. A blackbody source corrected for atmospheric absorption was assumed. The results are presented in Figs. 5 and 6. These maximum brightness temperatures are lower limits to the maximum interior gas temperatures because the fireball is optically thick. At early times the fireballs are nearly isothermal, thus the temperatures sensed may actually be the peak interior temperatures. At later times, the temperature of the cloud's interior is obscured by the cooler and optically thick exterior. The brightness temperatures observed by the two cameras for both events are in excellent agreement, suggesting that thermal continuum emission rather than line or band emission was observed.

IV. YAQUI CALCULATIONS

YAQUI, a LASL-developed computer program,[1,2] is used to solve the nonviscous hydrodynamic equations in cylindrical geometry. A computing grid with general quadrilateral cells is defined. Velocity components are defined at the cell vertices, whereas state variables (mass density, specific internal energy, pressure, etc.) are defined at the cell centers. Each computational cycle advances the solution in three steps or phases. Phase 1 provides an explicit Lagrangian solution of the mass and momentum conservation equations. The second phase performs an iteration to advance the pressure accelerations to the advanced time level. This procedure eliminates the usual Courant-like time-step criterion that restricts sound wave propagation to less than one cell width and replaces it with an accuracy criterion that only requires that material not move more than one cell width. The third phase allows the computing grid to be reconfigured. If the new vertex positions are different from those

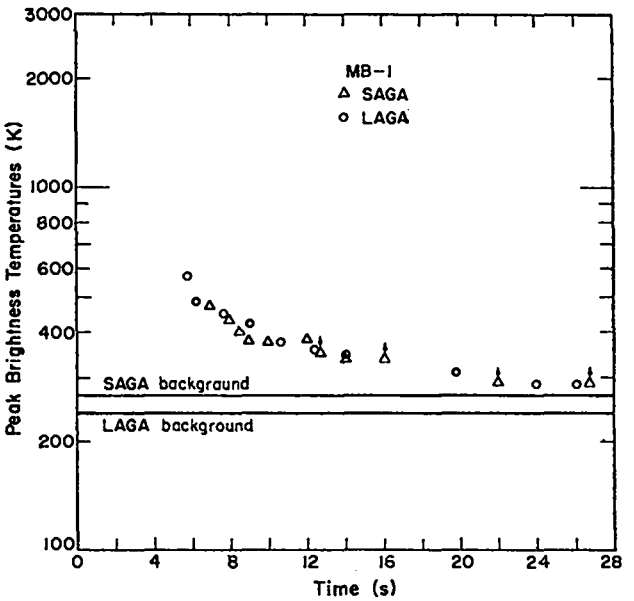

Fig. 5. Brightness temperatures derived from infrared cameras for MB-1.

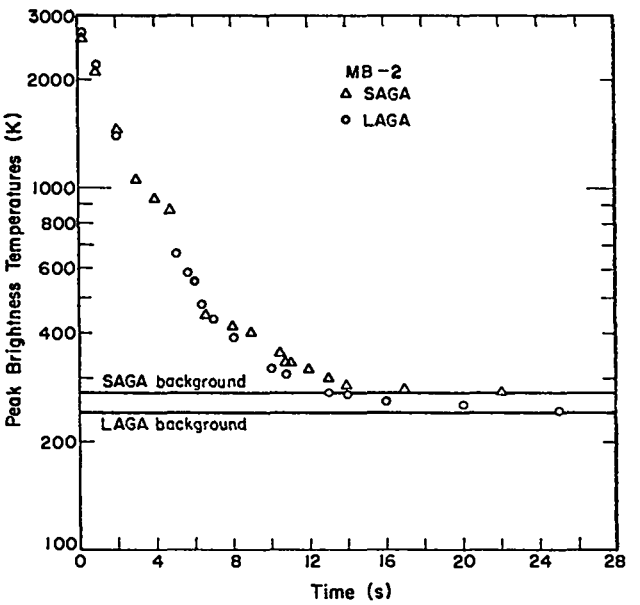

Fig. 6. Brightness temperatures derived from infrared cameras for MB-2.

resulting from the Lagrangian calculations of Phase 2, convective fluxes are computed to explain the transfer of mass, momentum, and energy between adjacent cells.

Captain Matuska, AFWL, supplied results of a one-dimensional calculation of the methane-oxygen explosion.[3] These results were used to define initial conditions. The initial YAQUI mesh had 10 cells across the fireball diameter. Velocity components, specific internal energies, and mass densities were interpolated from Matuska's results[3] to the appropriate positions in the YAQUI mesh. Ideally, one should use a two-fluid method to differentiate air from the explosion products. In this case, however, two single-fluid calculations were performed, one using the equation of state appropriate to air and one to explosion products everywhere in the mesh. Comparison of results showed no appreciable geometry differences, but substantial temperature differences. An AFWL two-fluid calculation[3] shows similar geometric results. The results presented below are from the calculation using the explosion-product equation of state.

The observed geometric results are described in Sec. II (Figs. 1 and 2). The agreement between the theoretical predictions of marker-material location and the visible data is extraordinary.

YAQUI calculates specific internal energy rather than temperature. Figure 7 shows the maximum predicted temperatures obtained using a c_v-table for a CO_2 and H_2O mixture to convert the calculated specific internal energy to temperature. The infrared peak brightness temperatures described in Sec. III are also shown. After detonation, the fireball is thought to be well-approximated by an isothermal sphere, and the brightness temperature and maximum temperature should be identical. There is excellent agreement between the computed postdetonation maximum temperature and the MB-2 data. At later times, various effects (noted in Sec. III) make the brightness temperature a lower limit to the fireball temperature. The YAQUI results are even lower than the lower limit brightness temperatures, indicating that either the calculation suffered numerical diffusion or the equation of state used was too simple.

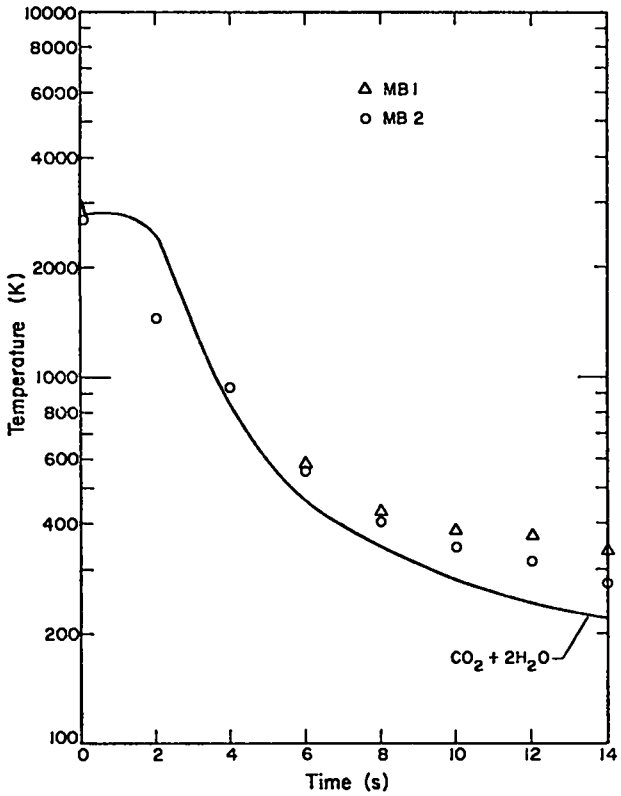

Fig. 7. Brightness temperatures for MB-1 and MB-2 from infrared records compared with calculated temperatures.

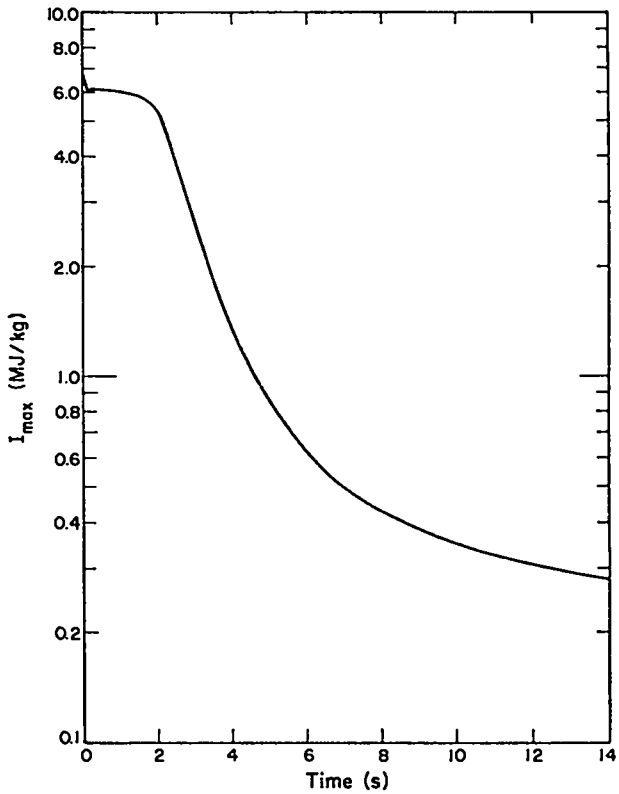

Fig. 8. Maximum specific internal energy from YAQUI calculation.

Figure 8 shows the maximum specific internal energy history. Comparison with other calculations shows that the breakup of the top of the fireball is marked by a sharp change in slope of the I_{max} curve; for the GEST experiments, this time is 2 s. We note that the peak temperature gradient is a lower limit at 18 K/cm. This value is near the peak mean gradient measured by the TRW hot-wire anemometer experiment.[4]

REFERENCES

1. A. A. Amsden and C. W. Hirt, "YAQUI: An Arbitrary Lagrangian-Eulerian Computer Program for Fluid Flow at All Speeds," Los Alamos Scientific Laboratory report LA-5100 (March 1973).

2. C. W. Hirt, A. A. Amsden, and J. L. Cook, "An Arbitrary Lagrangian-Eulerian Computing Method for All Flow Speeds," J. Comput. Phys. 14, 227-253 (1974).

3. Captain Dan Matuska, Air Force Weapons Laboratory, personal communication, 1974.

4. Richard Batt, TRW, personal communication, 1974.

APPENDIX

OPTICAL AND INFRARED IMAGES

Near-infrared (Mitchell camera), 5-μm (SAGA), and 10.5-μm (LAGA) images of MB-1 (Figs. A-1-A-6) and MB-2 (Figs. A-7-A-12) are presented. All pictures were reproduced at a 1 mm = 1 m scale at the source. Slight pointing differences from camera to camera result in slightly different centering of the clouds.

Brightness differences between the SAGA and LAGA images at a given time for one event were caused by camera adjustment rather than source differences. The peak brightness temperatures at 5 and 10.5 μm are virtually identical (see Sec. III). Also, the LAGA and SAGA images show similar structures.

As discussed in Sec. III, LAGA and SAGA detected self-luminous gas, whereas the visible and near-infrared cameras detected scattered sunlight. At all times, there is considerable similarity between the SAGA, LAGA, and near-infrared records. However, at late times there are "thin wisps" in the visible records that are hot and also "dense regions" that are cool. Intuition might suggest that "thin wisps" should be cool and "dense regions" hot.

There are considerable differences between the MB-1 and MB-2 clouds. By 6 s, the SAGA and LAGA records show that MB-1 had formed a well-defined, tilted vortex ring. There is some evidence in the records at 15 s that MB-2 had begun to form a torus, however it soon began to disperse. At 30 s, MB-1 still displayed a highly organized flow field.

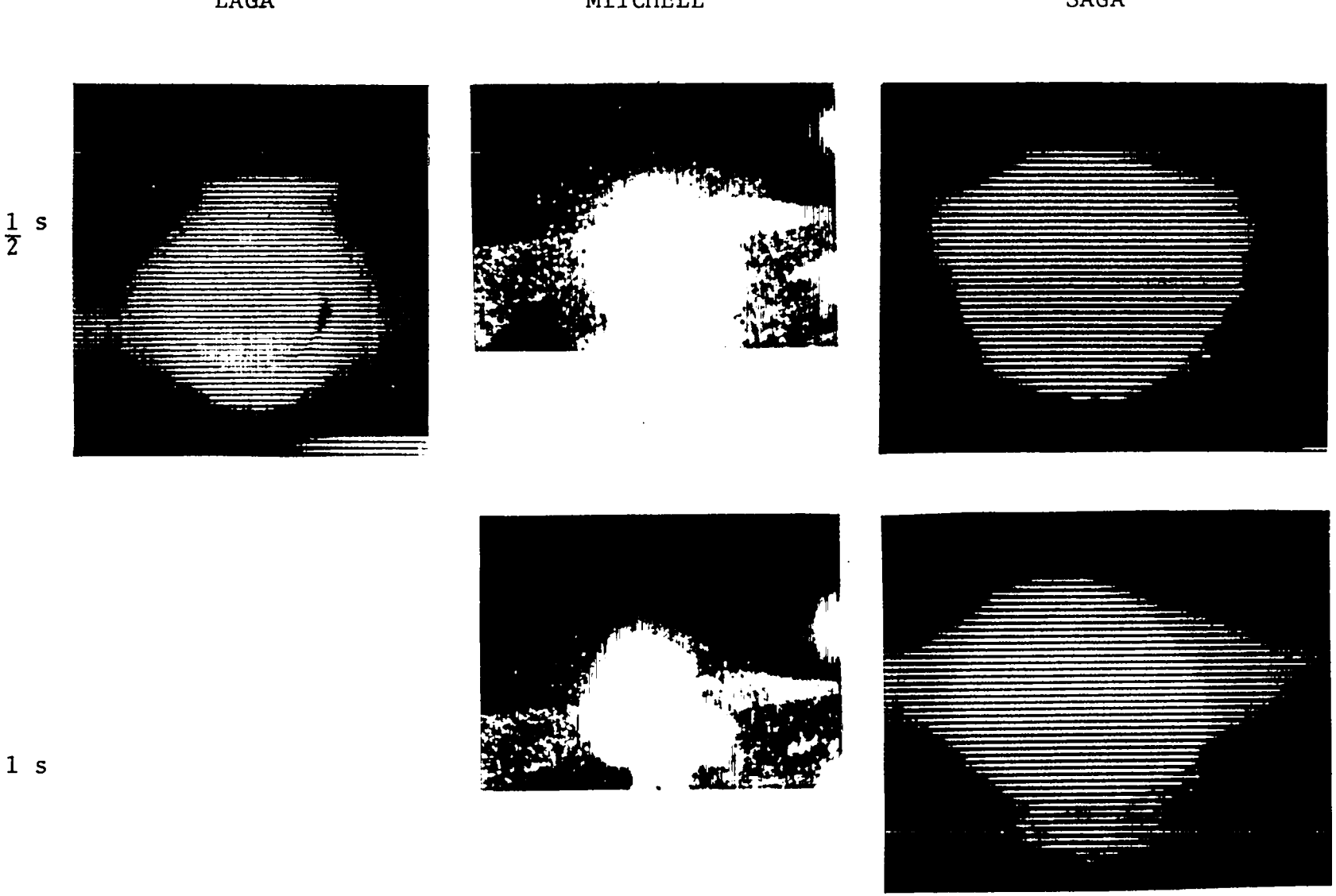

Fig. A-1. MB-1 Experiment. Infrared and near-infrared images at T+$\frac{1}{2}$ and T+1 s.

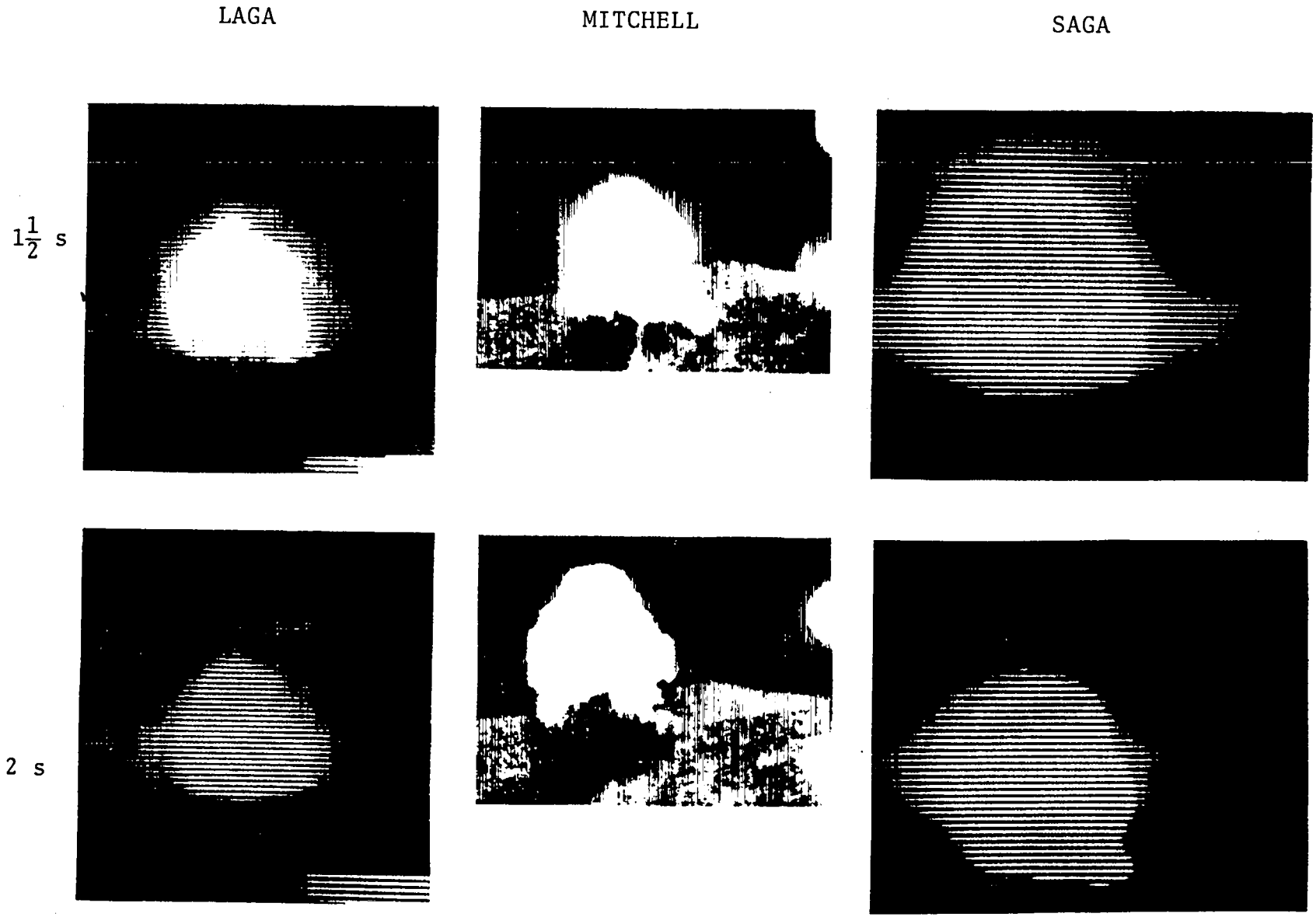

Fig. A-2. MB-1 Experiment. Infrared and near-infrared images at T+1½ and T+2 s. s.

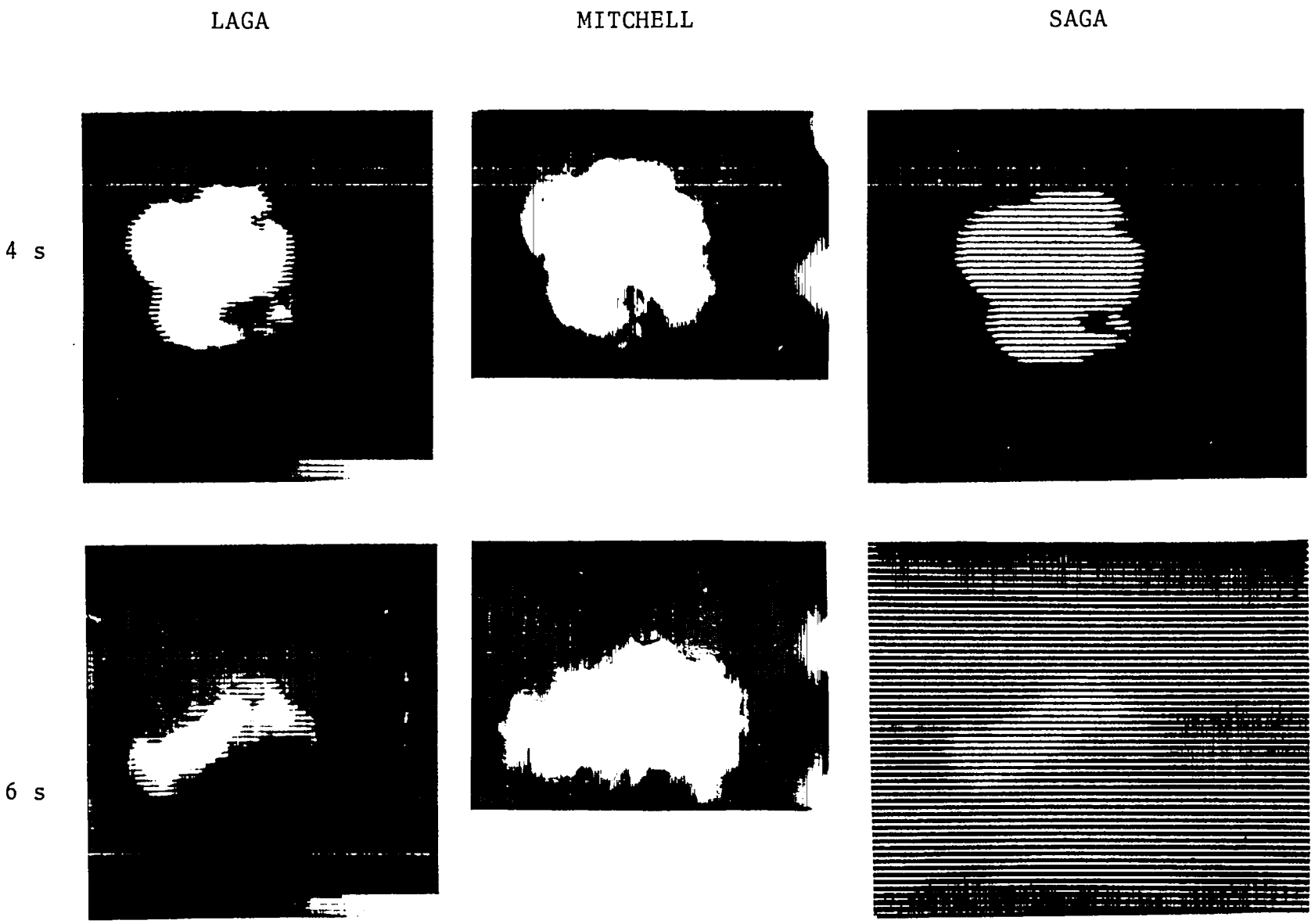

Fig. A-3. MB-1 Experiment. Infrared and near-infrared images at T+4 and T+6 s.

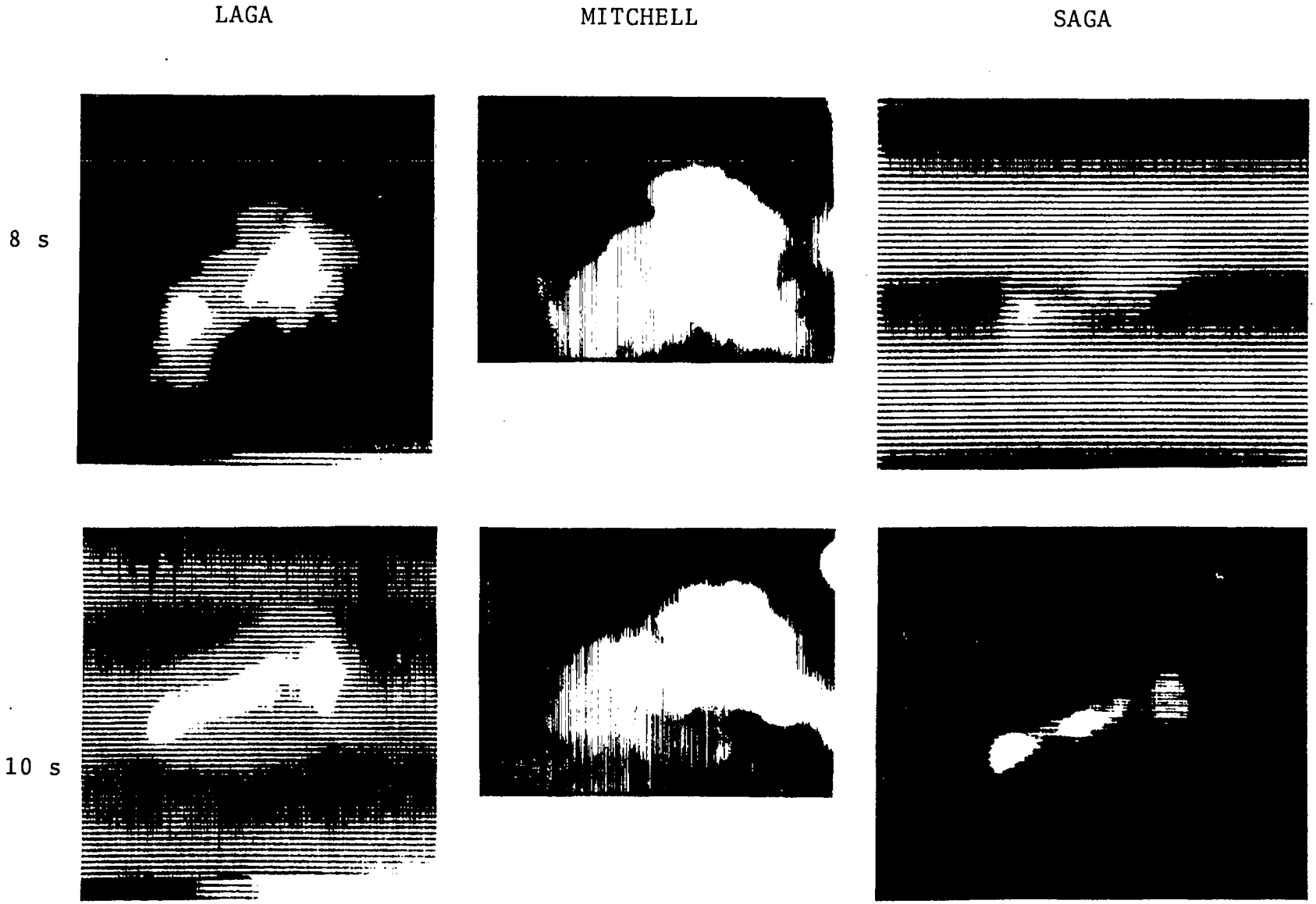

Fig. A-4. MB-1 Experiment. Infrared and near-infrared images at T+8 and T+10 s.

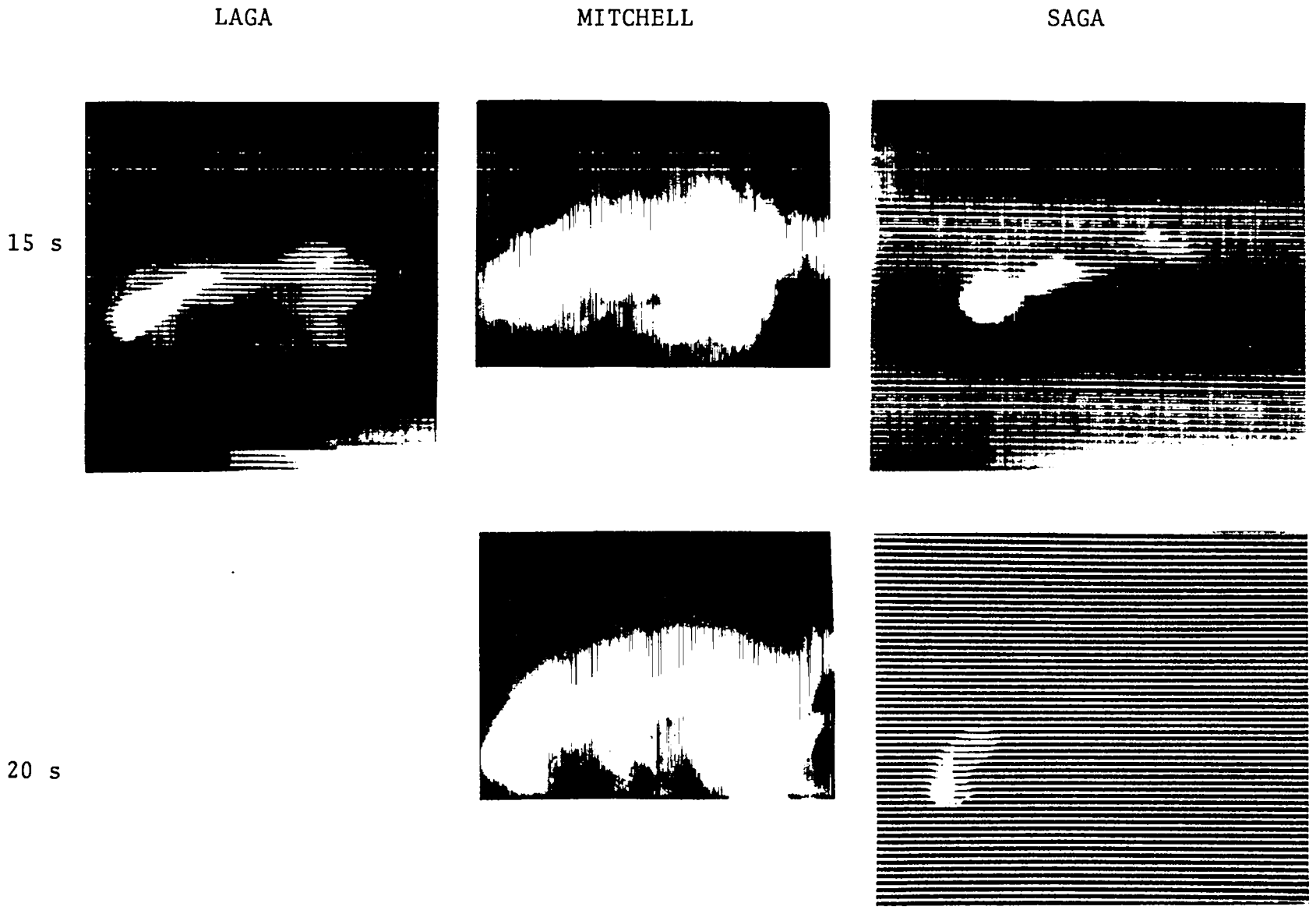

Fig. A-5. MB-1 Experiment. Infrared and near-infrared images at T+15 and T+20 s.

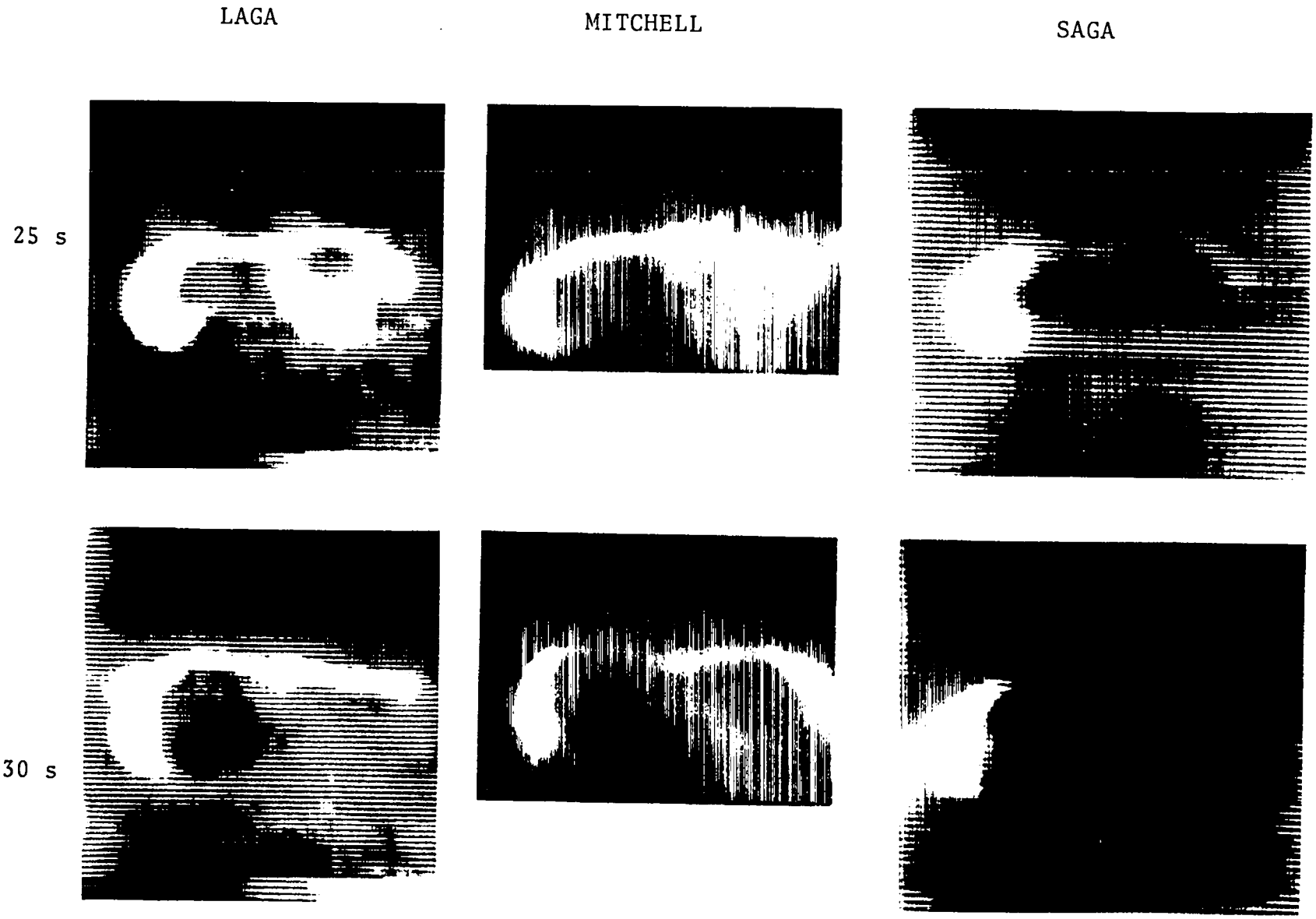

Fig. A-6. MB-1 Experiment. Infrared and near-infrared images at T+25 and T+30 s.

LAGA MITCHELL SAGA

$\frac{1}{2}$ s

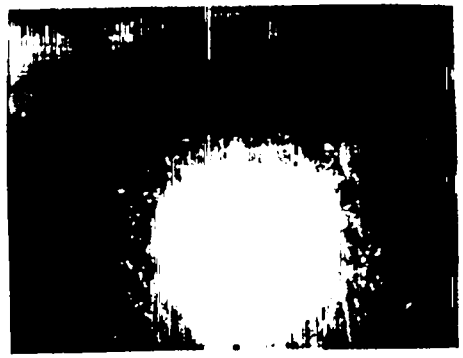

1 s

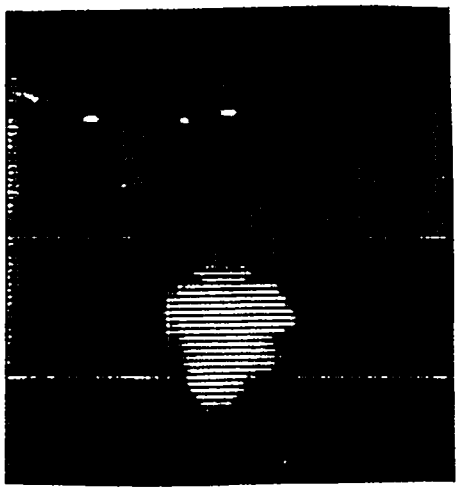

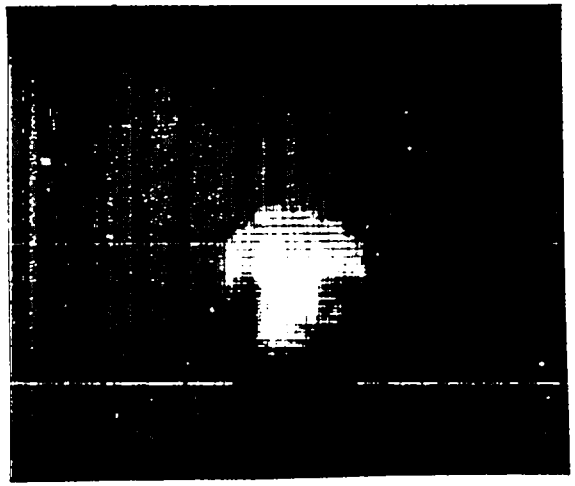

Fig. A-7. MB-2 Experiment. Infrared and near-infrared images at T+$\frac{1}{2}$ and T+1 s.

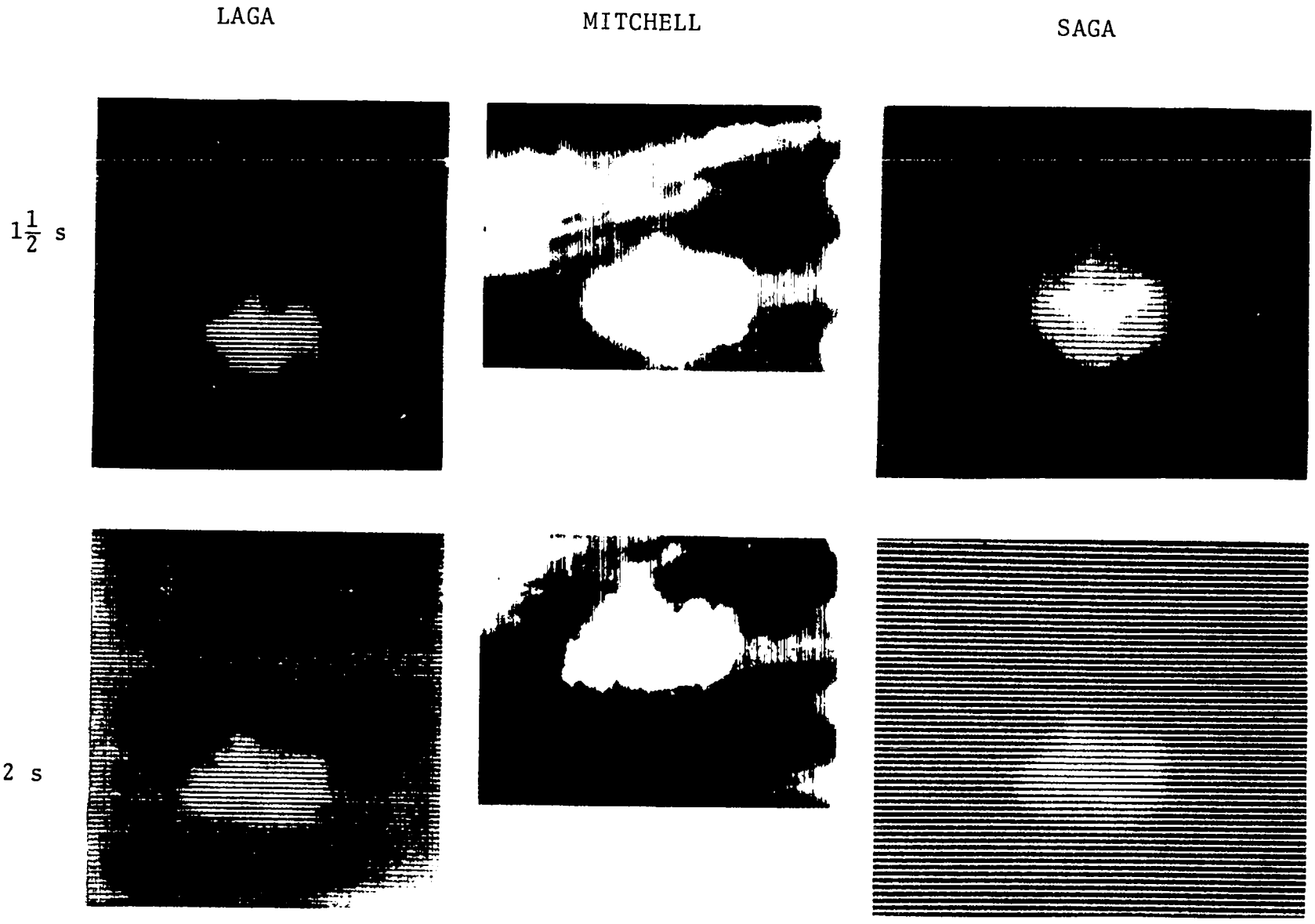

Fig. A-8. MB-2 Experiment. Infrared and near-infrared images at T+1$\frac{1}{2}$ and T+2 s.

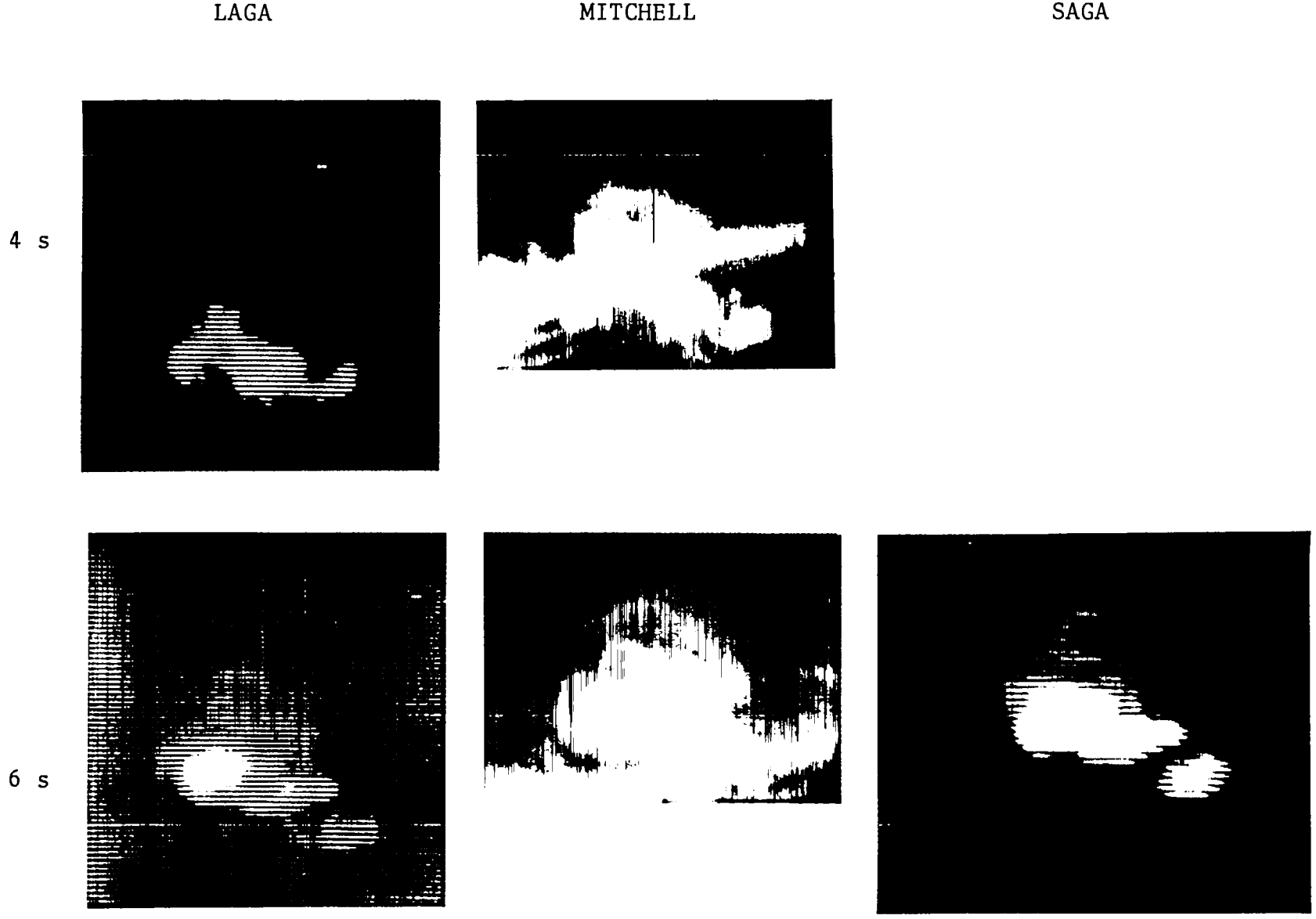

Fig. A-9. MB-2 Experiment. Infrared and near-infrared images at T+4 and T+6 s.

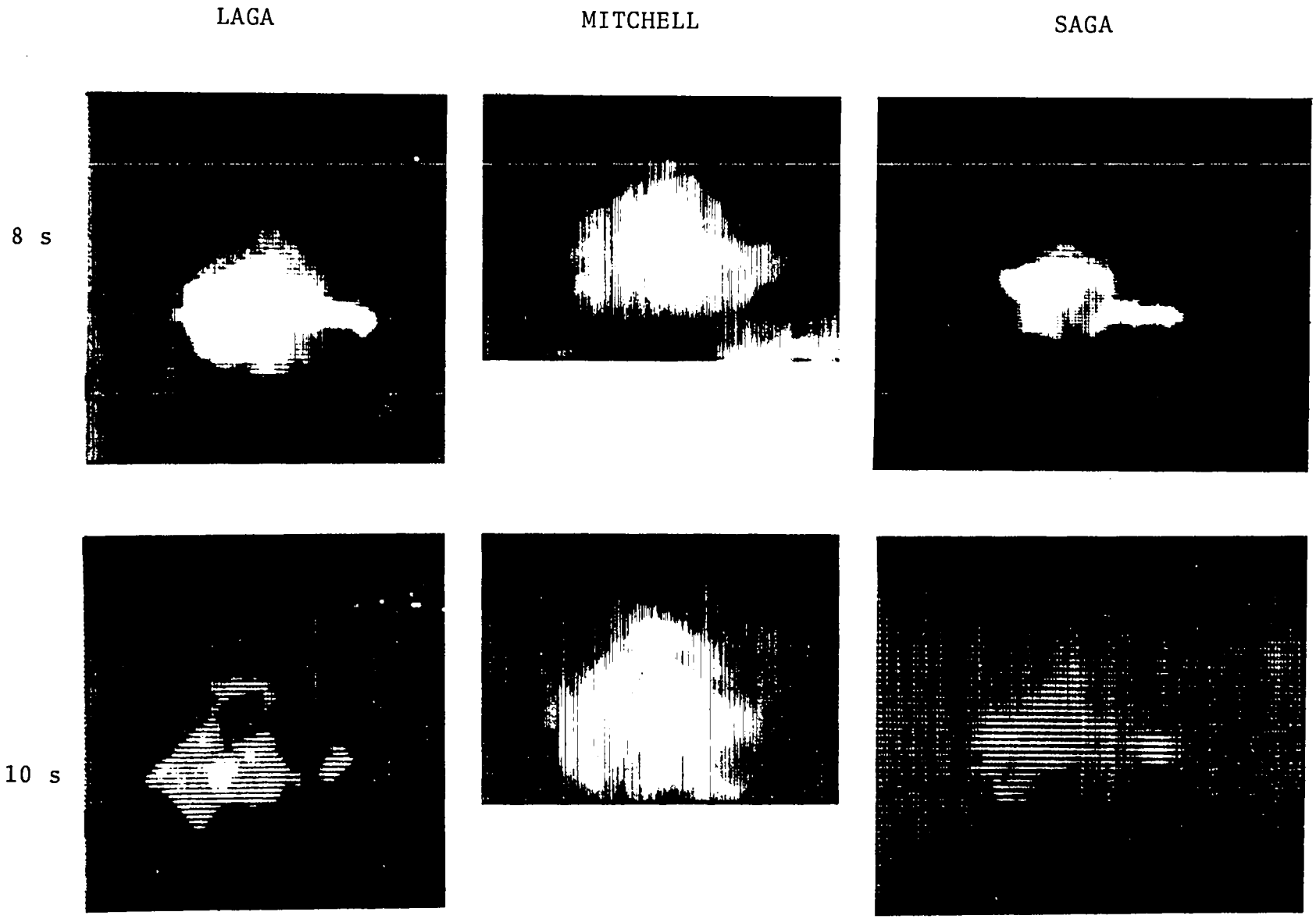

Fig. A-10. MB-2 Experiment. Infrared and near-infrared images at T+8 and T+10 s.

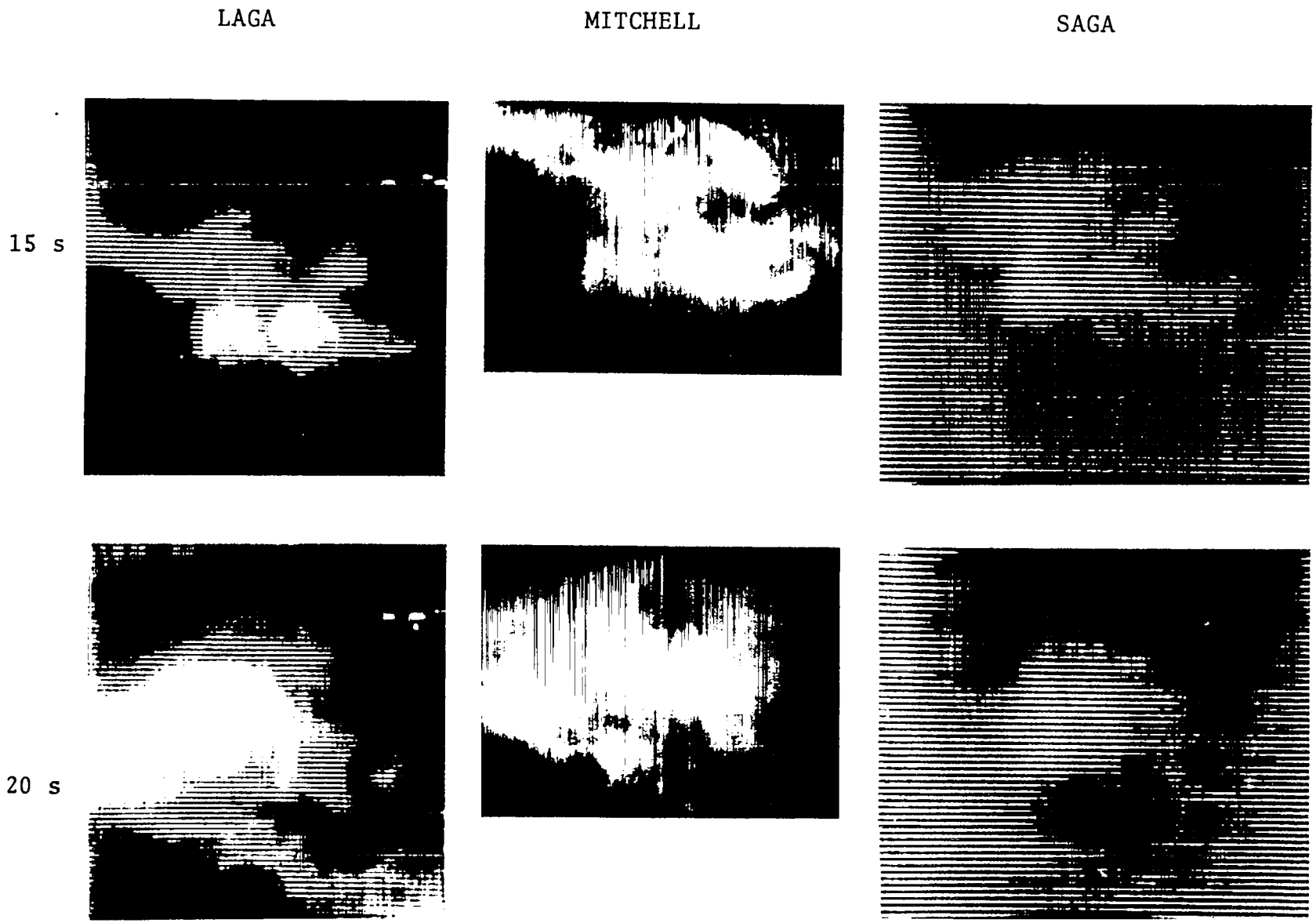

Fig. A-11. MB-2 Experiment. Infrared and near-infrared images at T+15 and T+20 s.

LAGA MITCHELL SAGA

25 s

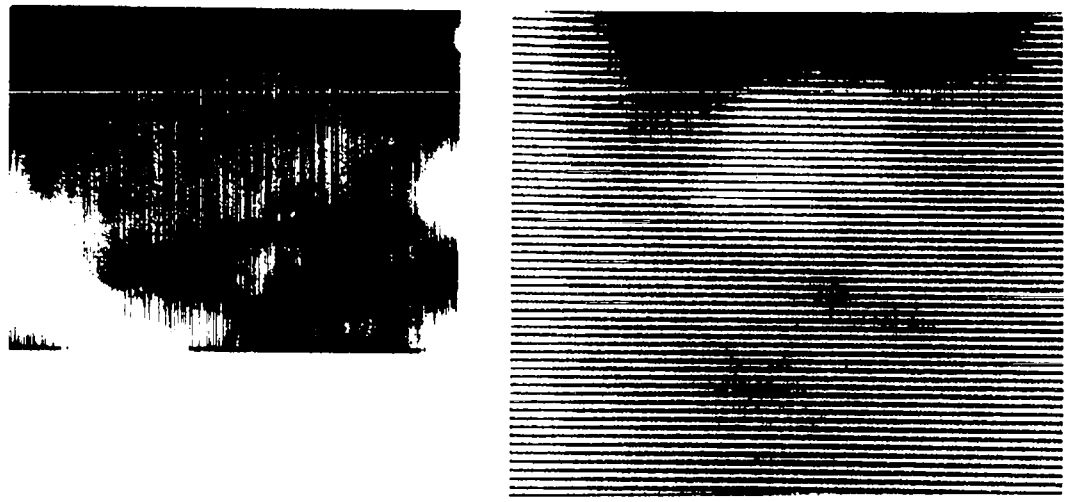

30 s

Fig. A-12. MB-2 Experiment. Infrared and near-infrared images at T+25 and T+30 s.